Materials Science and Engineering C 33 (2013) 4923–4934

Contents lists available at ScienceDirect

Materials Science and Engineering C

journal homepage: www.elsevier.com/locate/msec

Curcumin containing monoolein aqueous dispersions: A preformulative study

Elisabetta Esposito [a,*], Laura Ravani [a], Paolo Mariani [c], Catia Contado [d], Markus Drechsler [e], Carmelo Puglia [b], Rita Cortesi [a]

[a] Department of Life Sciences and Biotechnology, University of Ferrara, I-44121 Ferrara, Italy
[b] Department of Drug Sciences, University of Catania, I-95125 Catania, Italy
[c] Department of Life and Environmental Sciences and CNISM, Università Politecnica delle Marche, I-60100 Ancona, Italy
[d] Department of Chemistry, University of Ferrara, I-44121 Ferrara, Italy
[e] Macromolecular Chemistry II, University of Bayreuth, Germany

ARTICLE INFO

Article history:
Received 11 June 2013
Received in revised form 24 July 2013
Accepted 13 August 2013
Available online 27 August 2013

Keywords:
Monoolein
Cubosomes
Curcumin
Cryo-Transmission Electron Microscopy
Sedimentation Field Flow Fractionation
Franz cell

ABSTRACT

The present study describes the production and characterization of monoolein aqueous dispersions (MAD) as drug delivery systems for curcumin (CR).
MAD based on monoolein and different emulsifiers have been produced and characterized. Morphology and dimensional distribution have been investigated by Cryogenic Transmission Electron Microscopy (cryo-TEM), X-ray and Photon Correlation Spectroscopy (PCS).
Monoolein in different mixtures with sodium cholate, sodium caseinate, bentonite and poloxamer resulted in heterogeneous dispersions constituted of unilamellar vesicles, cubosomes and sponge type phases, depending on the employed components, as found by cryo-TEM and X-ray studies. CR was encapsulated with entrapment efficiencies depending on the MAD composition, particularly the highest was reached in the case of monoolein/poloxamer/sodium cholate mixture. The same mixture was able to maintain CR stability also after 6 months.
CR release modalities were in vitro investigated in order to mimic a possible subcutaneous administration of MAD. It was found that MAD constituted of monoolein/poloxamer and monoolein/poloxamer/sodium cholate mixtures were able to sustain CR release.
MAD viscous vehicles were produced by xanthan gum.
CR percutaneous absorption has been studied in vitro using excised human skin membranes [stratum corneum epidermis (SCE)] mounted into Franz cells. It was found that fluxes (F_n) of CR incorporated in MAD are influenced by the presence of monoolein based nanosystems. In particular xanthan gum based MAD better control CR diffusion from MAD.

1. Introduction

Curcumin (CR) is the chief component of the spice turmeric and is derived from the rhizome of the East Indian plant *Curcuma longa* [1]. CR is the principal curcuminoid and comprises approximately 2–5% of turmeric; it is responsible for the yellow colour of the spice as well as the majority of turmeric's therapeutic effects [2,3]. Aside from being employed as a flavouring and colouring agent in food, turmeric has also been widely used in Ayurvedic medicine for its anti-oxidant, antiseptic, analgesic, antimalarial and anti-inflammatory properties [4]. CR has been consumed as a dietary supplement for centuries and is considered pharmacologically safe. It is a suppressor of autoimmune diseases, including multiple sclerosis, type I diabetes, inflammatory bowel disease, systemic lupus erythromatosis, and myasthenia gravis [3]. Since CR protects skin by quenching free radicals and reducing inflammation through nuclear factor-KB inhibition, it has a beneficial role in skin diseases such as scleroderma, psoriasis and skin cancer (i.e. basal cell carcinoma) [5]. Moreover it is also well established that CR reduces wound-healing time, improves collagen deposition and increases fibroblast and vascular density in wounds [6].

Notwithstanding its numerous therapeutic effects, CR is difficult to administrate due to its scarce water solubility (clog P 3.2, PubChem CID969516). To overcome this drawback, advanced delivery strategies have been proposed, including nanoparticulate delivery systems such as liposomes, solid lipid microparticles, and cyclodextrins [7].

Lipid dispersions have a potential as matrixes able to dissolve and deliver active molecules in a controlled fashion, thereby improving

Abbreviations: MAD, monoolein aqueous dispersions; CR, curcumin; SdFFF, Sedimentation Field Flow Fractionation; cryo-TEM, Cryo-Transmission Electron Microscopy; SCE, stratum corneum epidermis.

* Corresponding author at: Dipartimento SVEB, Via Fossato di Mortara, 19, I-44100 Ferrara, Italy. Tel.: +39 0532 455259; fax. +39 0532 455953.
E-mail address: ese@unife.it (E. Esposito).

0928-4931/$ – see front matter © 2013 Elsevier B.V. All rights reserved.
http://dx.doi.org/10.1016/j.msec.2013.08.017

their bioavailability and reducing side-effects [8–10]. Unsaturated long-chain monoglycerides emulsified in water lead to aqueous nanostructured dispersions of complex lyotropic liquid crystalline phases (lamellar, hexagonal, and cubic) [11–14]. In particular, it has been observed that both structure and stability of the dispersed phase are influenced by the emulsifier [15,16]. The role of emulsifier is central: on one side, its nature influences the nanostructure and the stability of the disperse phases [8] on the other, it can lead to enhanced solubilisation of poorly water-soluble drugs. One of the more used surfactant is the Poloxamer 407 copolymer, which shows thermoreversible characteristics of the utmost interest in optimizing drug formulation. Poloxamer 407 is able to emulsify monoolein in water, giving rise to the formation of aqueous dispersions mainly constituted of a mixture of cubosomes, hexasomes and vesicles [9,12,14,17].

This study describes the production and characterization of monoolein aqueous dispersions (MAD) as drug delivery systems for CR.

In the present case, monoolein was used in mixture with poloxamer and with different emulsifiers of natural origin, such as sodium cholate, sodium caseinate and bentonite, in order to investigate natural materials as alternative to poloxamer in the production of MAD.

Characterization studies were then performed: cryo-TEM and X-ray studies were used to shed light on the morphology and the inner structure of the MAD produced using different emulsifiers, whereas dimensional distributions of the dispersed particles were determined by Photon Correlation Spectroscopy and Sedimentation Field Flow Fractionation. A stability study was conducted in order to explore the capability of MAD in controlling CR degradation. The in vitro CR release was studied in order to mimic subcutaneous administration of MAD.

In the last part of the study an in vitro screening was performed in order to investigate the suitability of MAD for dermatological application.

To this aim MAD viscosity has been improved by xanthan gum, then Franz cell coupled with excised human skin membranes [stratum corneum epidermis (SCE)] were employed to compare the diffusion kinetics of CR from the different MAD.

2. Materials and methods

2.1. Materials

Glyceryl monooleate RYLO MG 19 (monoolein) was a gift from Danisco Cultor (Grindsted, Denmark). Pluronic F127 (Poloxamer 407, poloxamer) (PEO_{98}-POP_{67}-PEO_{98}) was obtained from BASF (Ludwigshafen, Germany). Curcumin (CR), (1E,6E)-1,7-bis(4-Hydroxy-3-methoxyphenyl)-1,6-heptadiene-3,5-dione, sodium cholate (Na cholate) (3α,7α,12α-Trihydroxy-5β-cholan-24-oic acid sodium salt), sodium caseinate (Na caseinate) (αS1, αS2, β, κ) and bentonite (aluminium phyllosilicate, montmorillonite) were purchased from Sigma Chemical Company (St Louis, MO, USA). Solvents were of HPLC grade and all other chemicals were of analytical grade.

2.2. MAD preparation

Production of dispersions was based on the emulsification of monoolein and emulsifier in water, as previously described [14]. MAD compositions are reported in Table 1.

After emulsification, the dispersions were subjected to homogenization (15,000 rev min^{-1}, Ultra Turrax, Janke & Kunkel, Ika-Werk, Sardo, Italy) at 60 °C for 1 min, then they were cooled and maintained at room temperature in glass vials.

In the case of CR containing MAD, 7.5 mg of CR (0.33% w/w with respect to the monoolein, 0.015% w/w with respect to the dispersion) was added to the molten monoolein/emulsifier mixture and dissolved before addition to the aqueous solution. During production the vial was protected from light with an aluminium foil to prevent photodegradation of CR.

2.3. Characterization of lipid dispersions

2.3.1. Cryo-Transmission Electron Microscopy (Cryo-TEM)

Samples were vitrified as described in a previous study [14]. The vitrified specimen was transferred to a Zeiss EM922Omega (Carl Zeiss Microscopy, Oberkochen, Germany) transmission electron microscope using a cryoholder (CT3500, Gatan, Munich, Germany). Sample temperature was kept below 100 K throughout the examination. Specimens were examined with reduced doses of about 1000–2000 e/nm^2 at 200 kV. Images were recorded by a CCD digital camera (Ultrascan 1000, Gatan, Munich, Germany) and analysed using a GMS 1.8 software (Gatan, Munich, Germany).

2.3.2. X-ray diffraction measurements

X-ray diffraction experiments were performed using a 3.5 kW Philips PW 1830 X-ray generator (Amsterdam, Netherlands) equipped with a Guinier-type focusing camera (homemade design and construction, Ancona, Italy) operating in vacuum with a bent quartz crystal monochromator ($\lambda = 1.54$ Å). Diffraction patterns were recorded on GNR Analytical Instruments Imaging Plate system (Novara, Italy). Samples were held in a tight vacuum cylindrical cell provided with thin

Table 1
Composition of MAD[a].

# MAD	MAD composition (% w/w)						Notes
	Monoolein	Na cholate	Na caseinate	Bentonite	Poloxamer 407	H_2O	
1	4.5	–	–	–	0.5	95.00	Milky stable dispersion with few aggregates
2	4.5	0.15	–	–	0.5	94.85	Translucent stable dispersion
3	5	0.1	–	–	–	94.90	Transparent dispersion
4	5	0.25	–	–	–	94.75	Foamy transparent dispersion
5	4.5	0.15	–	–	–	95.35	Transparent dispersion with some aggregates
6	4.5	0.25	–	–	–	95.25	Almost transparent dispersion
7	4.5	–	0.15	–	–	95.35	Translucent dispersion Creaming
8	4.5	–	0.25	–	–	95.35	Translucent dispersion Creaming
9	5	–	0.25	–	–	94.75	Translucent dispersion Creaming
10	5	–	–	0.5	–	94.50	Phase separation
11	4.5	–	–	0.5	–	95.00	Phase separation
12	4.5	0.15	–	0.5	–	94.85	Grey milky stable dispersion
13	4.5	–	0.15	0.5	–	94.85	Milky dispersion with some aggregates
14	4.5	0.15	0.1	–	–	94.25	Almost milky dispersion with some aggregates
15	4.5	0.15	0.07	–	–	95.28	Milky dispersion with few aggregates

[a] Monoolein aqueous dispersion.

mylar windows. Diffraction data were collected at three different temperatures of 25, 37 and 45 °C.

In each experiment, a number of Bragg peaks was detected in the low-angle region and the peak indexing was performed considering the different symmetries commonly observed in lipidic phases [18]. Once the lattice symmetry was derived, the unit cell dimension, *a*, was calculated from the averaged spacing of the observed peaks. The disordered nature of the short-range lipid conformation was confirmed by analysing the high-angle X-ray diffraction profiles [11].

2.3.3. Photon correlation spectroscopy (PCS)

Submicron particle size analysis was performed using a Zetasizer 3000 PCS (Malvern Instr., Malvern, England) equipped with a 5 mW helium neon laser with a wavelength output of 633 nm. Glassware was cleaned of dust by washing with detergent and rinsing twice with sterile water. Measurements were made at 25 °C at an angle of 90° with a run time of at least 180 s. Samples were diluted with bidistilled water in a 1:10 v:v ratio. Data were analysed using the "CONTIN" method [19].

2.3.4. Sedimentation Field Flow Fractionation analysis

A Sedimentation Field Flow Fractionation (SdFFF) system (Model S101, FFFractionation, Inc., Salt Lake City, UT, USA), described elsewhere [14], was employed to determine the size distribution of particles (PSD) by converting the fractograms, i.e. the graphical results, assuming that the particle density is known [20]. The mobile phase was a 0.01% v/v solution of FL-70 in Milli-Q water (Millipore S.p.A., Vimodrone, Milan, Italy) pumped at 1.0 ml/min and monitored in each run. Fifty microliter samples were injected as they were through a 50 μl Rheodyne loop valve.

The fractions were automatically collected after the SdFFF system by a Model 2110 fraction collector (BioRad laboratories, UK) with a collecting time of 90 s. The volume of each fraction was 3 ml.

2.4. Drug content of dispersions

SdFFF was employed to obtain information about CR encapsulation and its distribution in the dispersions. During the fractionation, some fractions were collected and analysed by HPLC to quantify the amount of drug contained in the different particle populations of the disperse phase. CR encapsulation values in MAD were obtained by summing the amount of CR in the different fractions.

CR encapsulation efficiency was also determined as previously reported [21] by diluting an amount of MAD with ethanol (1:10, v/v) and stirring for 3 h at 0 °C in an amber glass bottle in order to prevent CR degradation. A filtered sample was then analysed by HPLC for CR content.

All data were the mean of four determinations on different batches of the same type of dispersion. Chemical stability was evaluated on drug loaded formulations, which were stored at 25 °C in amber glass bottle for 6 months, determining CR content by HPLC analyses after 30, 90 and 180 days.

2.5. Gel production

MAD have been viscosized by adding xanthan gum (1% w/w) directly into the dispersion and by slowly stirring for 1 h, until complete dispersion of the gum.

2.6. Rheology study

Viscosity values of xanthan gum gel in the absence (x gum) and in the presence of MAD (MAD-x gum) were measured by a Brookfield dial reading viscometer model RTV (Brookfield engineering laboratories, Stoughton, MA, USA). Appropriate spindles with different speeds (0.1–5 rev/min) were used to obtain the correct dial readings. Three readings were taken for each sample, and the mean dial reading was corrected using factors supplied by the instrument manufacturer.

2.7. In vitro release kinetics of curcumin from MAD

In vitro release studies were performed using modified Franz diffusion cell. Dialysis membrane having a pore size of 2.4 nm and a molecular weight cutoff between 12,000 and 14,000 was used. Membrane was soaked in double-distilled water for 12 h before mounting in a Franz diffusion cell. MAD (1 ml) was placed in the donor compartment and the receptor compartment was filled with 5 ml of a mixture of phosphate buffer 60 mM pH 7.4 and methanol (50:50, v/v) to allow the establishment of the sink conditions and to sustain permeant solubilization [22]. A magnetic bar stirred the mixture at 500 rpm, and the system was thermostated at 37 ± 1 °C. At fixed time intervals, 100 μl of the sample was withdrawn from the receiver compartment through the side tube. Fresh receiving mixture was placed to maintain constant volume. Samples were analysed by HPLC method as described below. The CR concentrations were determined four times in independent experiments and the mean values ± standard deviations were calculated.

2.8. Drug release data analysis

The experimental release data obtained with both methods were then fitted to the following semiempirical equations respectively describing Fickian dissolutive and diffusional release mechanisms [23]:

$$Mt/M\infty = K_{Diss}t^{0.5} + c \quad (1)$$

$$1 - Mt/M\infty = e^{-K_{Diff}t} + c \quad (2)$$

where $Mt/M\infty$ represents the drug fraction released at the time t ($M\infty$ is the total drug content of the analysed amount of MAD), K and c are coefficients calculated by plotting the linear forms of the indicated equations. The release data up to the plateau of percent of released drug were used to produce theoretical release curves.

2.9. In vitro percutaneous absorption studies

2.9.1. Skin membrane preparation

Samples of adult human skin (mean age 36 ± 8 years) were obtained from breast reduction operations. Subcutaneous fat was carefully trimmed and the skin was immersed in distilled water at 60 ± 1 °C for 2 min [24], after which SCE were removed from the dermis using a dull scalpel blade. Epidermal membranes were dried in a desiccator at ~25% relative humidity. The dried samples were wrapped in aluminium foil and stored at 4 ± 1 °C until use. Previous research works demonstrated the maintenance of SC barrier characteristics after storage in the reported conditions [24,25]. Besides, preliminary experiments were carried out in order to assess the barrier integrity of SCE samples by measuring the in vitro permeability of [^{3}H] water through the membranes using the Franz cell method described below. The value of calculated permeability coefficient for [^{3}H] water agreed well with those previously reported [26].

2.9.2. In vitro skin permeation experiments

Samples of dried SCE were rehydrated by immersion in distilled water at room temperature for 1 h before being mounted in Franz-type diffusion cells supplied by LGA (Berkeley, CA).

The exposed skin surface area was 0.78 cm^2 (the diameter of the orifice was 1 cm). The receptor compartment contained 5 ml of a mixture of phosphate buffer 60 mM pH 7.4 and methanol (50:50, v/v) as reported above. This solution was stirred with the help of a

magnetic bar at 500 rpm and thermostated at 32 ± 1 °C during all the experiments [27].

Approximately 500 μl of each formulation was placed on the skin surface in the donor compartment and the latter was sealed to avoid evaporation. At predetermined time intervals comprised between 1 and 24 h, samples (0.15 ml) of receptor phase were withdrawn and CR concentration in the receptor phase was measured using HPLC. Each removed sample was replaced with an equal volume of simple receptor phase. The CR concentrations were determined six times in independent experiments and the mean values ± standard deviations were calculated. The mean values were then plotted as a function of time. The diffusion coefficients, computed from the linear portion of the accumulation curve, represent the experimentally observed fluxes (F_o).

Normalized fluxes F_n were then calculated by the following equation:

$$F_n = F_o/C \quad (3)$$

where C is the CR concentration (in mg/ml) in the analysed form.

2.10. HPLC procedure

HPLC determinations were performed using a two-plunger alternative pump (Jasco, Japan), an UV-detector operating at 425 nm, and a 7125 Rheodyne injection valve with a 50 μl loop. Samples were loaded on a stainless steel C-18 reverse-phase column (15 × 0.46 cm) packed with 5 μm particles (Grace® — Alltima, Alltech, USA).

Elution was performed with a mobile phase containing methanol, 2% acetic acid and acetonitrile 5:30:65 v/v at a flow rate of 0.5 ml/min. The retention time of CR was 7.0 min.

2.11. Statistical analysis

Statistical analysis of data was performed using the Student's-test. A probability, p, of less than 0.05 is considered significant in this study.

3. Results and discussion

3.1. Characterization of dispersions

A preformulative study was conducted in order to select some MAD for CR encapsulation. Fifteen MAD have been produced, based on the use of the above reported emulsifiers, alone or in mixture. In particular besides the synthetic poloxamer, naturally derived materials were employed, namely Na cholate (the bile salt commonly used for liposome production), casein (the major protein present in milk), and bentonite (a clay mineral).

Table 1 reports the compositions of the produced MAD, together with some comments about appearance and stability of the dispersions.

One can observe that poloxamer allowed the obtainment of milky stable dispersions with few aggregates, while Na cholate resulted in the production of transparent dispersions. In particular foamy transparent dispersions were obtained using the highest content of both monoolein and Na cholate (MAD # 4).

The mixture of Na cholate and poloxamer gave rise to a translucent dispersion.The use of Na caseinate led to production of dispersions with an initial translucent appearance followed by creaming, otherwise when Na caseinate was used together with Na cholate, milky dispersions with few aggregates were formed.

Finally bentonite used alone led to phase separation, while if employed together with Na cholate or Na caseinate, allowed the formation of milky dispersions with some aggregates.

Five MAD (namely # 1, 2, 4, 12 and 15) have been chosen to study their potential as CR delivery systems, considering as selection criteria the absence of separation phenomena and the scarceness of aggregates. The selected MAD have been renamed by acronyms based on their compositions: MP (monoolein and poloxamer 407), MC (monoolein and Na cholate), MCP (monoolein, Na cholate and poloxamer 407), MCC (monoolein, Na cholate and Na caseinate), and MCB (monoolein, Na cholate and bentonite).

After producing the selected MAD in the presence of CR, the visual aspect was again evaluated. It was found that CR doesn't affect the macroscopic appearance of dispersions, apart from the change of colour from white to yellow.

It is noteworthy that, apart from MCC where some aggregates formed, CR, due to its amphiphilic character, concurs to stabilize MAD, preventing formation of aggregates. Indeed the presence of aggregates after MP production was found [14]. The method used to determine the weight of the aggregates and their CR content in MCC is reported in the “Supplementary data” section.

3.1.1. Cryo-TEM analyses

Cryo-electron transmission microscope analyses were conducted in order to investigate the internal structures of MAD and to compare the emulsifier influence on the nanostructure of the disperse phase. Figs. 1 and 2 report cryo-TEM images of MAD produced by different emulsifiers. In panels A and B of Fig. 1, images of MP dispersions in the absence and in the presence of CR are respectively reported. In both panels the coexistence of vesicles and cubosomes can be observed. Cubosomes appear as well-shaped particles with a homogeneous, ordered inner structure. Some cubosomes show vesicles attached on their surface. In addition sponge-like cubic systems are present. The images show that the typical structures found for MAD constituted of monoolein and poloxamer [8,17].

Conversely, in the case of MC (panels C and D) and MCP (panels E and F), unilamellar vesicles are present. The black points are ascribed to ice crystal contamination due to sample preparation. The presence of CR doesn't seem to affect MAD aspect. From cryo-TEM images it can be asserted that the use of Na cholate as emulsifier, alone or in mixture with poloxamer, doesn't allow the formation of cubic or sponge-like structures but only of unilamellar vesicles. Nevertheless other authors have found that monoolein in dilute micellar bile salt solutions forms vesicles and different liquid crystalline phases [28,29].

Fig. 2 shows images of MCC (panels A and B) and MCB (panels C and D). In Fig. 2A, referred as plain MCC, mixtures of vesicles, cubosomes and hexasomes can be seen. The vesicles are mainly unilamellar or show some invaginations, besides some very large membrane systems such as sponge-type cubic structures can be observed. Fig. 2B concerns a sample of a dispersion produced in the presence of CR (CR-MCC). Here, the vesicles showing the invaginations are mixed with some hexasomes in different formation states. Casein, being an amphiphilic protein, exhibits self-association into micellar aggregates in water; its capability to form cubosomes in the presence of monoolein has been previously demonstrated by other authors [30–32]. With regard to MCB dispersion, different structures can be noted. In Fig. 2C, referred as plain MCB, cubosomes, sponge structures and vesicles can be detected. The dark lines are thin bentonite sheets (ca. 1 nm) in side view.

Finally Fig. 2D, concerning CR-MCB, shows a heterogeneous system constituted of vesicles with invaginations, sponge-type phase particles and bentonite platelets in side view, looking like needles. The arrow points a vesicle with an invagination (the channel can be seen on top and left side) with cubic structure in the centre. The sponge phase is probably built from these invaginations and develops further to the cubic phase. Moreover, in the same sample, cubosomes, unilamellar vesicles and huge areas of cubic phase membrane systems are present (images not shown).

The cryo-TEM observations of Fig. 2 enable to assert that the emulsification of monoolein by Na cholate in mixture with Na

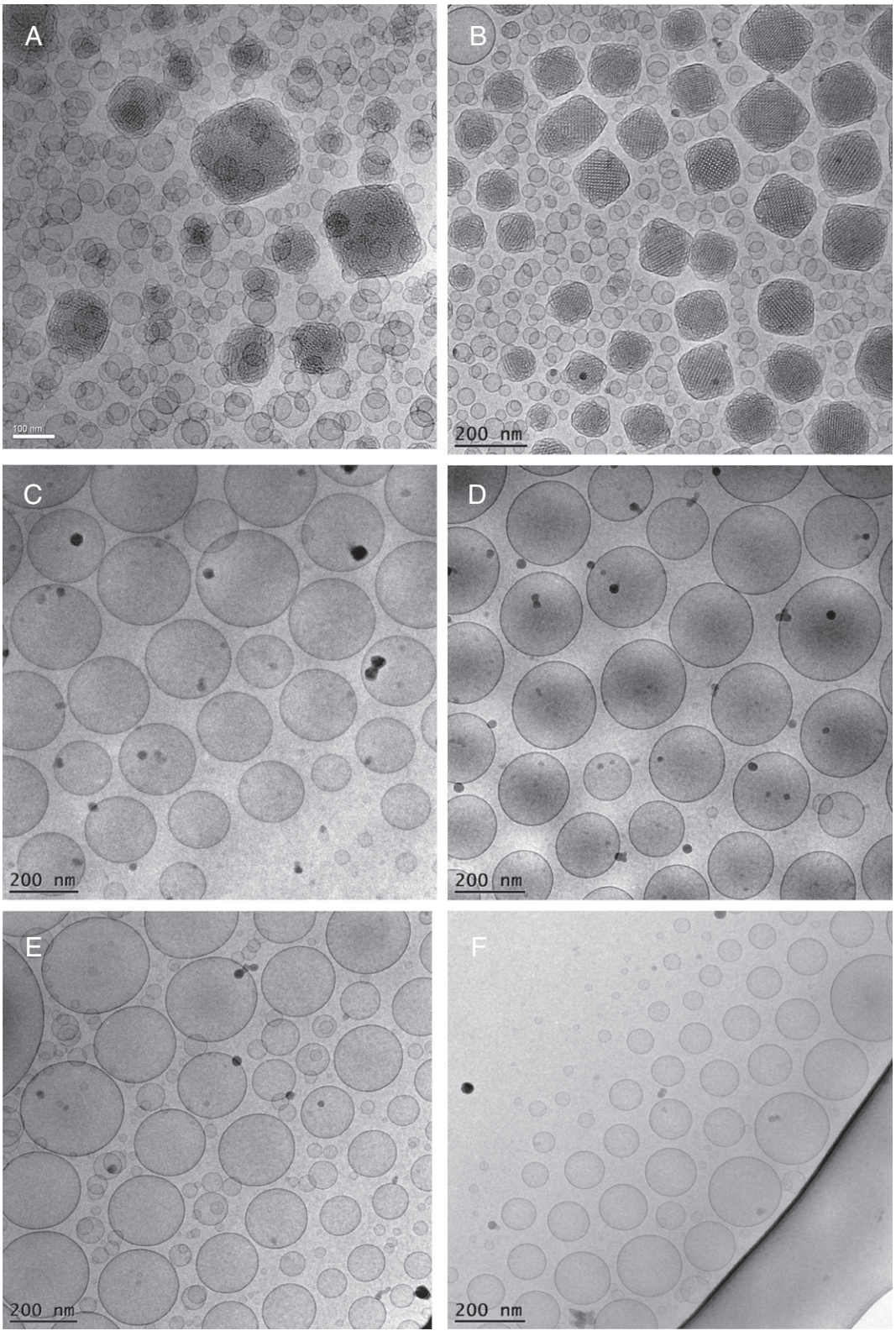

Fig. 1. Cryo-transmission electron microscopy images (cryo-TEM) of MAD produced in the absence and in the presence of CR. MAD were stabilized by different emulsifiers, namely poloxamer 407 (MP) (panels A, B), Na cholate (MC) (panels C, D) and Na cholate–poloxamer 407 (MCP) (panels E, F). Panels B, D and F refer to CR containing MAD.

caseinate or with bentonite allows the formation of cubic, sponge-like structures and vesicles with invaginations. The presence of CR seems to affect the MAD nanostructures, in fact, due to its amphiphilic nature [33], and CR behaves as a surfactant that interacts with monoolein in the formation of different crystalline structures.

3.1.2. X-ray diffraction analyses

X-ray diffraction was used to investigate the inner structural organization of MAD. Experiments were performed as a function of temperature on different MAD preparations, both in the presence and in the absence of CR. Few examples of X-ray diffraction results

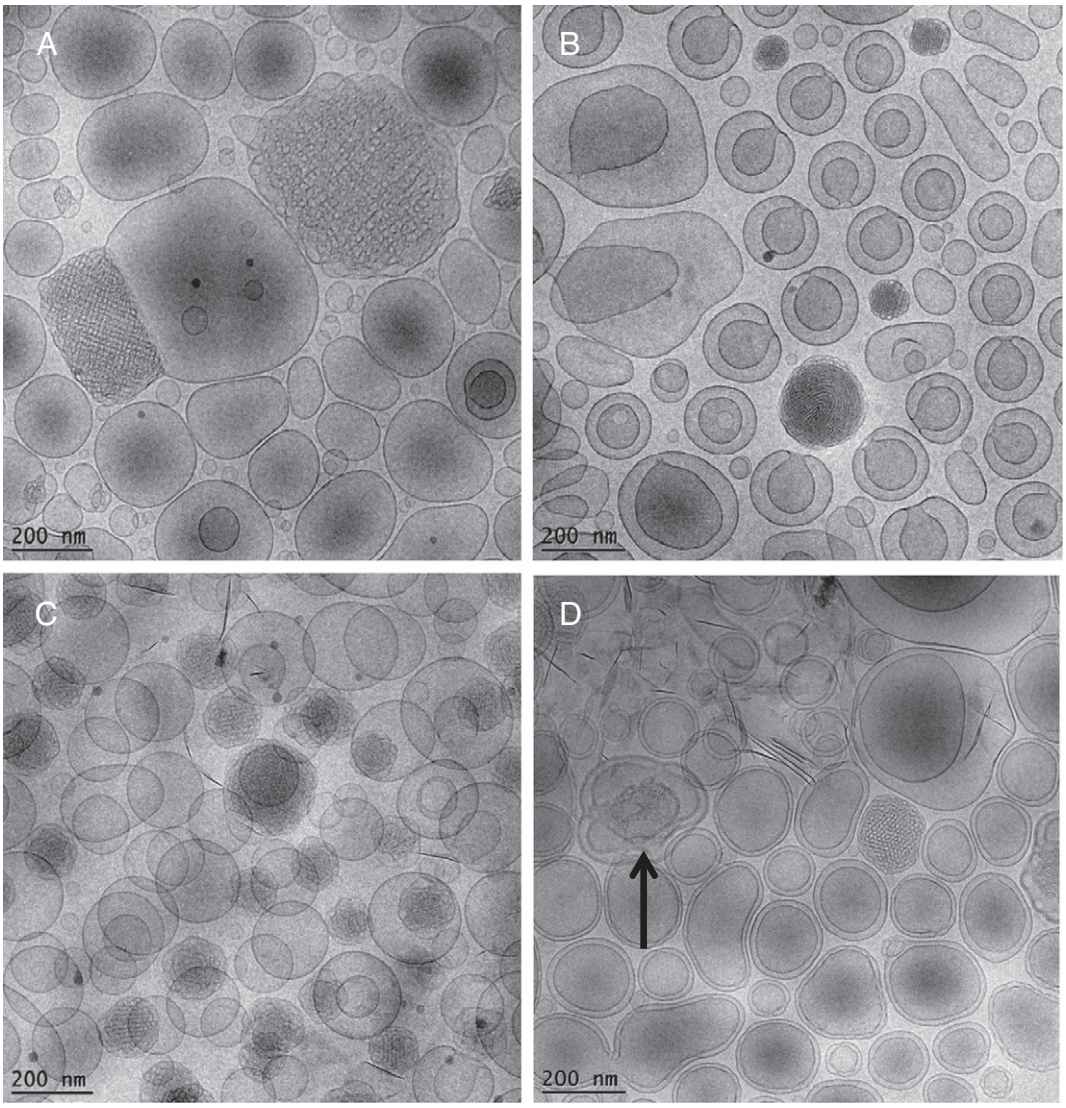

Fig. 2. Cryo-transmission electron microscopy images (cryo-TEM) of MAD produced in the absence and in the presence of CR. MAD were stabilized by different emulsifiers, namely Na cholate–Na caseinate (MCC) (panels A, B) and Na cholate–bentonite MCB (panels C, D). Panels B and D refer to CR containing MAD.

are shown in Fig. 3. It can be observed that the diffraction pattern changes with composition and temperature, indicating phase transitions (i.e. CR-MCB sample, in which temperature induces transition from *Pn3m* to *H* phase) or simple modifications of the unit cell dimensions (i.e. CR-MCC and CR-MP, in which the changes in peak positions indicate an increase of the unit cell dimension by increasing temperature). Whole results are summarized in Table 2. As a general comment, it can be observed that MAD preferentially show a *Pn3m* inner structure (the bicontinuous cubic structure formed by monoolein in excess of water at room temperature), even if heating process can induce the phase transition to a 2D hexagonal structure. Compared with pure monoolein in excess water [19], emulsifiers appear to induce a small dehydration of the cubic structure (a reduction of the unit cell dimension from the reference value of 104 Å is systematically observed), while the addition of CR slightly increases the unit cell dimensions. Due to the amphiphilic nature, CR probably promotes an increase of the negative curvature of the polar/apolar interface, thus inducing a larger unit cell and a consequent stabilization of the cubic phase.

Considering the data reported in Table 2, the singular cases in which Na Cholate is used should be noticed. In particular, MAD stabilized by Na Cholate (sample MC) show only a low-angle diffuse scattering, indicating that internal order is absent (e.g., presence of unilamellar vesicles) or limited to very small regions. However, the addition of CR (sample CR-MC) induces the restructuring of MAD, which are characterized by a stable bicontinuous *Pn3m* cubic inner structure. On the other side, MAD prepared using Na cholate in mixture with poloxamer results in formation of *Pn3m* cubosomes both in the absence and in the presence of CR (samples MCP and CR-MCP). Such results are in agreement with the above reported observations by Lindstrom and colleagues [28], but data apparently disagree with cryo-TEM analyses, since cryo-TEM images of CR-MC, MCP and CR-MCP samples only show the presence of vesicles (Fig. 1, panels D, E and F). In this regard it should be underlined that in few cases inner structured cubosomes or hexasomes could not be trapped during freezing processes, mostly it should be observed that only a very small volume of the sample is examined by TEM. By contrast, a very large sample volume is analysed by X-ray diffraction, and even small amounts of ordered phases can be easily detected. Therefore, the whole results for CR-MC, MCP and CR-MCP suggest the contemporaneous presence of vesicles and inner structured particles.

When Na caseinate is included in monoolein/Na cholate MAD preparations (sample MCC), the main formation of a thermally stable hexagonal structure is detected. In such a case, the addition of CR (sample CR-MCC) does not induce phase transitions: MAD inner structure remains hexagonal at all the investigated temperatures.

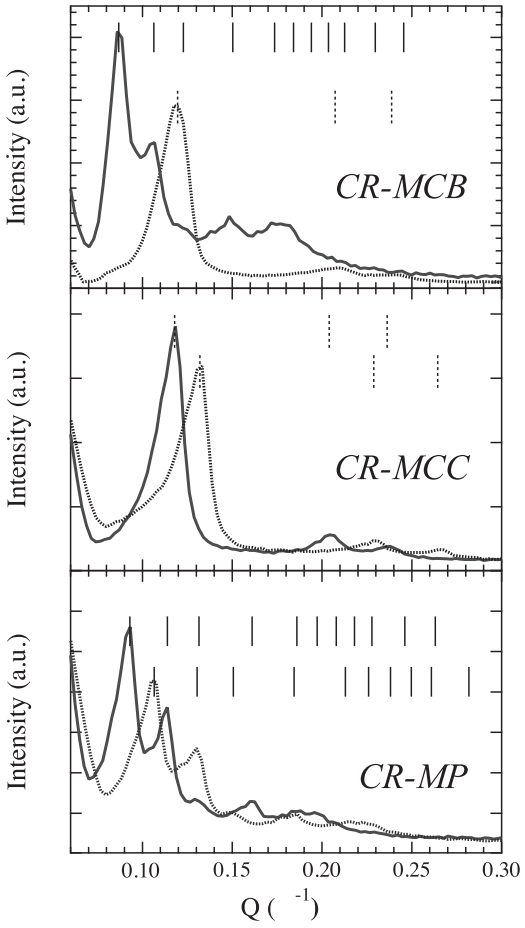

Fig. 3. Typical X-ray diffraction profiles observed at different temperatures for the considered MAD. The sample acronym is reported in the frame, while continuous and dotted lines indicate profiles obtained at 25 and 45 °C, respectively. Bars indicate the peak positions calculated for the different phases (black bars: *Pn3m*; dotted bars: *H*). Note that the first bar is superimposed to the first observed peak. The corresponding unit cells are reported in Table 3.

Finally, MAD emulsified by Na cholate and bentonite (sample MCB) show an unstable bicontinuous *Pn3m* cubic structure, which transforms in a hexagonal phase under heating and which maintains the same characteristic after CR addition (sample CR-MCB). In this case the presence of different structural organizations (including cubosomes, hexasomes and unilamellar vesicles) was also detected by cryo-TEM observations.

3.1.3. PCS analyses

PCS studies were conducted to determine the dimensional distribution of MAD dispersions, Table 3 reports the typical parameters obtained by PCS after production of differently composed samples of CR-MAD. Mean diameters expressed as Z average are comprised between 153.5 (when MAD is emulsified by Na cholate and poloxamer, MCP) and 235.5 nm (when Na cholate is employed together with bentonite, MCB). The analyses by volume revealed bi-dimensional distributions of MAD, apart from that stabilized by Na cholate and poloxamer. Polydispersity indexes are always below 0.3.

Fig. 4 summarizes the mean results obtained on MAD produced in the absence and in the presence of CR.

As reported in panel A, MAD mean intensity diameters range between 158.9 nm, for MCP and 252.97 nm for MCB. MP and MC have almost superimposable mean diameters, being 208.7 and 206.9 nm respectively. The use of Na cholate associated to poloxamer (MCP) results in a decrease of mean diameter with respect to the use of the sole poloxamer (MP), while the association of Na cholate with Na caseinate (MCC) or bentonite (MCB) leads to an increase of mean diameters. The presence of CR resulted in a slight decrease in mean diameter in all MAD, apart from MC, where the mean diameter doesn't change. The differences in mean diameters between the same formulation produced in the absence and in the presence of CR are statistically significant ($p < 0.0001$).

As shown in Fig. 4B, polydispersity indexes (PI) are always equal or below 0.4. The lowest PI values are obtained by MP, both in the absence and in the presence of CR, while MCP displays the highest PI in the absence of CR. The presence of CR induces an increase of PI values, apart from MCP, where PI decreases from 0.4 to 0.24 in the presence of the drug, passing from a bimodal to a monomodal distribution (data not shown). Finally MCB maintains the PI value of 0.34, which is also in the presence of CR.

3.1.4. SdFFF analyses

Size distribution was also determined by SdFFF. The fractograms obtained under the same separation conditions (to allow a direct comparison) were converted into PSD plots, i.e. the amount of material per unit change of diameter, according to well-proven equations, by transforming the retention time in a size, which is the diameter of a compact sphere having the sorted mass, and the UV signal into a mass frequency function [14,20]. Fig. 5 shows the PSD plots of CR-MAD produced by different emulsifiers, namely MP (panel A), MC (panel B), MCP (panel C), MCC (panel D), and MCB (panel E). The conversion was performed by assuming an average density of 0.9692 g/ml for all MAD.

As a general statement, all samples are characterized by bimodal PSDs that differ by the separation degree between the two components and their relative intensities. The presence of bimodal distributions is usually confirmed by PCS "analysis by volume", that is in agreement also in describing MCP (Fig. 5C), in which the second population appears in the SdFFF plot only as a shoulder just delineated on the right of the main peak. Indeed for MCP the average size determined by SdFFF is ~150 nm, which is in excellent agreement with the 130 nm measured with the PCS. In the case of MP (Fig. 5A), the SdFFF analysis

Table 2
Structural organization of MAD at different lipid compositions as derived by X-ray diffraction analysis.

Acronym	Lipid composition	Phase and unit cell (±0.5 Å) at 25, 37 and 45 °C		
MP	Monoolein/poloxamer 407	*Pn3m*, 91.1 Å	*Pn3m*, 87.6 Å	*Pn3m/H*, 87.1/60.0 Å
CR-MP	CR-monoolein/poloxamer 407[a]	*Pn3m*, 95.5 Å	*Pn3m*, 89.6 Å	*Pn3m*, 83.2 Å
MC	Monoolein/Na cholate	*Diffuse*	*Diffuse*	*Diffuse*
CR-MC	CR-monoolein/Na cholate[a]	*Pn3m*, 94.5 Å	*Pn3m*, 92.7 Å	*Pn3m*, 88.8 Å
MCP	Monoolein/Na cholate/poloxamer 407	*Pn3m*, 96.6 Å	*Pn3m*, 91.6 Å	*Pn3m*, 90.7 Å
CR-MCP	CR-monoolein/Na cholate/poloxamer 407[a]	*Pn3m*, 97.2 Å	*Pn3m*, 92.6 Å	*Pn3m*, 91.2 Å
MCC	Monoolein/Na cholate/Na caseinate	*H*, 54.6 Å	*H*, 54.1 Å	*H*, 53.3 Å
CR-MCC	CR-monoolein/Na cholate/Na caseinate[a]	*H*, 61.4 Å	*H*, 57.1 Å	*H*, 54.6 Å
MCB	Monoolein/Na cholate/bentonite	*Pn3m*, 93.5 Å	*Pn3m/H*, 83.4/62.0 Å	*H*, 61.0 Å
CR-MCB	CR-monoolein/Na cholate/bentonite[a]	*Pn3m*, 103.0 Å	*H*, 60.9 Å	*H*, 60.5 Å

[a] MAD produced in the presence of curcumin; CR: curcumin.

Table 3
Typical PCS parameters of CR-MAD[a] based on different compositions.

Parameter	MAD composition				
	Monoolein Poloxamer 407 (MP)	Monoolein Na cholate (MC)	Monoolein Na cholate Poloxamer 407 (MCP)	Monoolein Na cholate Na caseinate (MCC)	Monoolein Na cholate Bentonite (MCB)
Z average *mean diameter (nm)*	200.3	206.8	153.5	219.0	235.5
Analysis by intensity *mean diameter (nm)*	198.9	189.8	154.5	227.5	189.0
Analysis by volume *mean diameter (nm)*	151.3 (peak area 77.3%)	152.4 (peak area 86.5%)	131.5	150.4 (peak area 51.6%)	129.8 (peak area 80.9%)
	395.3 (peak area 22.7%)	393.2 (peak area 13.5%)		287.6 (peak area 48.4%)	409.1 (peak area 18.7%)
Analysis by number *mean diameter (nm)*	116.2 (peak area 99.3%)	118.2 (peak area 99.7%)	95.7	145.6 (peak area 88.2%)	96.6 (peak area 99.6%)
				270.1 (peak area 11.8%)	
Polydispersity index	0.26	0.27	0.29	0.28	0.25

[a] MAD produced in the presence of curcumin.

shows a bimodal distribution peaking at ~120 nm and 170 nm respectively, while cryo-TEM analyses show well structured cubic particles of about 130–200 nm, along with a number of smaller vesicles (Fig. 1B). It is plausible to assert, especially for this sample, that the unique density value, set for the fractogram conversion into PSD, cannot well represent the whole sample composition, bringing to possible equivalent spherical diameter values.

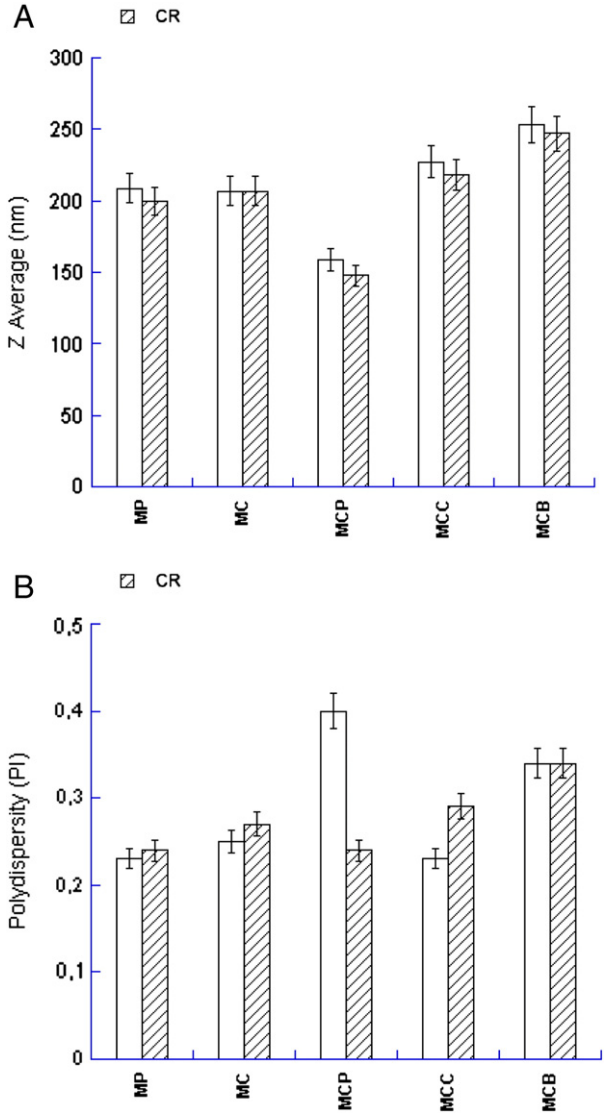

Fig. 4. Z average and polydispersity indexes (PI) of MAD produced in the absence (empty pattern) and in the presence of CR (diagonal line pattern), as indicated by the histograms. MAD were stabilized by different emulsifiers, namely poloxamer 407 (MP), Na cholate (MC), Na cholate–poloxamer 407 (MCP), Na cholate–Na caseinate (MCC) and Na cholate–bentonite (MCB). Data are the means of 5 analyses on different batches of the same type of dispersions.

For MC, dimensions sized by SdFFF were between 75 and 180 nm, with two prevalent sizes at ~110 nm and 150 nm (Fig. 5B), in agreement with the first population monitored by PCS (~150 nm). Since the PCS "analysis by number" attests the presence of a single population, it is likely to suppose, as done for MP, that the largest particles represent only negligible minority undetected by the SdFFF.

More articulated are the considerations on the PSDs of MCC and MCB, reported in Fig. 5D and E respectively. The bimodal PSD of MCC shows prevalent sizes at 130 nm and 160 nm; the two populations are the best distinct among all tested dispersions, even if the two peaks are still overlapped. On the other hand the PCS analysis confirms, either by volume and by number, the presence of two populations with mean diameters of ~150 nm and 280 nm. The disagreement between the results achieved with the two techniques appears meaningful, but it highlights the complexity of the particles achieved through this formulation. The cryo-TEM image reported in Fig. 2B well shows the presence of cubic, sponge-like structures and vesicles with invaginations, whose density is likely very heterogeneous, and not representable by a single value. At last the results achieved for MCB are the most difficult to be interpreted, since the PSD obtained by SdFFF resembles the PSD of MCC and the PCS results are accordingly in line with it. The heterogeneous population of MCC and MCB requires the conjunction of different techniques in order to interpret the obtained results.

3.2. Drug content of dispersions

SdFFF was employed to obtain information about CR encapsulation and its distribution in the dispersions. During the fractionation, some fractions were collected and analysed by HPLC to quantify the amount of drug contained in the different particle populations of the disperse phase [14].

Fig. 5 also reports the concentration of CR in each fraction determined by HPLC. It is evident that CR was entirely associated with particles in all MAD dispersions.

The drug distribution within the different fractions was similar for all MAD. Particularly the fraction corresponding to a mean diameter of about 70–80 nm (probably constituted by vesicles) contains 12–25% of the total drug. The highest amount of CR (48–60%) is contained in the most representative portion of nanoparticles/vesicles, having a diameter of about 100 nm. Particles with mean diameters of about 130 nm contains 7–18% of CR. The remaining CR is associated with the least representative population of particles, having larger diameter.

CR encapsulation values in MAD, obtained by summing CR concentration in the different fractions, are reported in the table of Fig. 5. CR encapsulation is almost quantitative for all MAD, with the

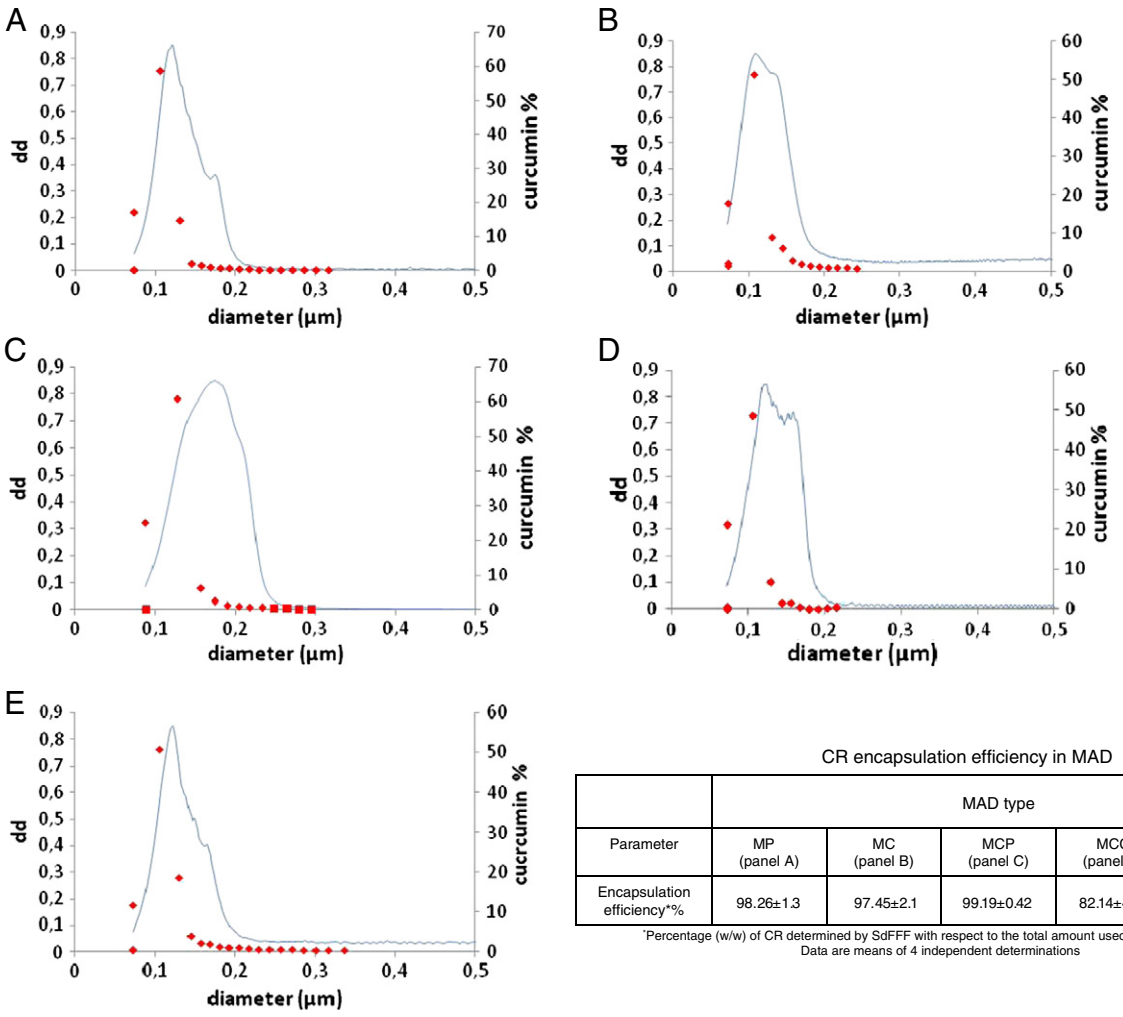

CR encapsulation efficiency in MAD

	MAD type				
Parameter	MP (panel A)	MC (panel B)	MCP (panel C)	MCC (panel D)	MCB (panel E)
Encapsulation efficiency*%	98.26±1.3	97.45±2.1	99.19±0.42	82.14±4.5	98.04±0.48

*Percentage (w/w) of CR determined by SdFFF with respect to the total amount used for the preparation. Data are means of 4 independent determinations

Fig. 5. MAD PSDs elaborated from the SdFFF fractograms and CR encapsulation efficiency values in MAD (reported in the table). MAD were stabilized by different emulsifiers, namely poloxamer 407 (MP, panel A), Na cholate (MC, panel B), Na cholate–poloxamer 407 (MCP, panel C), Na cholate–Na caseinate (MCC, panel D) and Na cholate–bentonite (MCB, panel E). MAD particles were assumed to have a density of 0.9692 g/ml (d = diameter of nanoparticles; dd = dimensional distribution; the dots indicate CR content, as determined by HPLC).

highest value obtained by MCP, followed by MP. The lowest recovery value is obtained in the case of MCC (82.14% w/w). The lost CR is found associated to the aggregates which are formed during MAD production (Supplementary data). CR encapsulation efficacy data, determined by MAD dilution in ethanol and stirring, were superimposable (data not shown). Apart the CR encapsulation difference between MCC and the other MAD, differences between CR encapsulation were not statistically significant.

Concerning CR stability, it should be underlined that the molecule in phosphate buffer 0.1 M is rapidly decomposed ($t_{1/2}$ = 9.4 min) [34]. The CR instability is due to degradation by acidic and alkaline hydrolysis, oxidation and photodegradation [35–37].

Fig. 6 reports the CR content in the different formulations as a function of time, expressed as percentage of the total amount used for the preparation. One can appreciate the differences in CR stability kinetics displayed by the MAD. In particular, MCP maintains CR stability better than the other MAD, in fact after 6 months from production the residual concentration of CR is still 98.3%. In the case of MP the residual CR content is 80.78%.

Our results show that the stability of CR in MAD seems to be influenced by pH (Table 5) as previously reported [38]. The lower the pH value, the higher the CR residual content after 6 months. In fact curcuminoids are known to be stable at pH below 6.5. They decompose in a pH-dependent manner, with faster reactions at neutral to basic conditions [36].

Concerning the macroscopic aspect, CR-MAD maintained their yellow colour and the almost absence of aggregates at least after six months from production.

3.3. In vitro drug release studies

The stability tests, showing a controllable CR degradation, suggest MCP and MP use for the long-term sustained releasing of drug. Moreover MCP and MP appear suitable for injection, having particle size in the range of 100–200 nm (Fig. 4). For these reasons the CR releasing mode from MCP and MP has been investigated.

Many research groups used vertical or flow-through Franz diffusion cells and dialysis bag/tubes for the study of drug release from colloidal lipid systems and polymeric nanoparticles [39–42]. Modified Franz diffusion cells with dialysis membrane were used in our study to mimic a subcutaneous administration. Dialysis membrane retained nanosystems and allowed the transfer of the drug immediately into the receiver compartment. Since CR is poorly soluble in aqueous media, the use of physiological media as receptor phases led to negligible diffusion kinetics. Hence a non-physiological receptor phase with 50% v/v of methanol was used [22].

Fig. 7A shows the percentage release of CR from MP and MCP. CR was released in a sustained manner from both MAD, with a slower kinetic in the case of MCP. Statistical analysis revealed significant differences ($p < 0.01$) between release values obtained for both MAD.

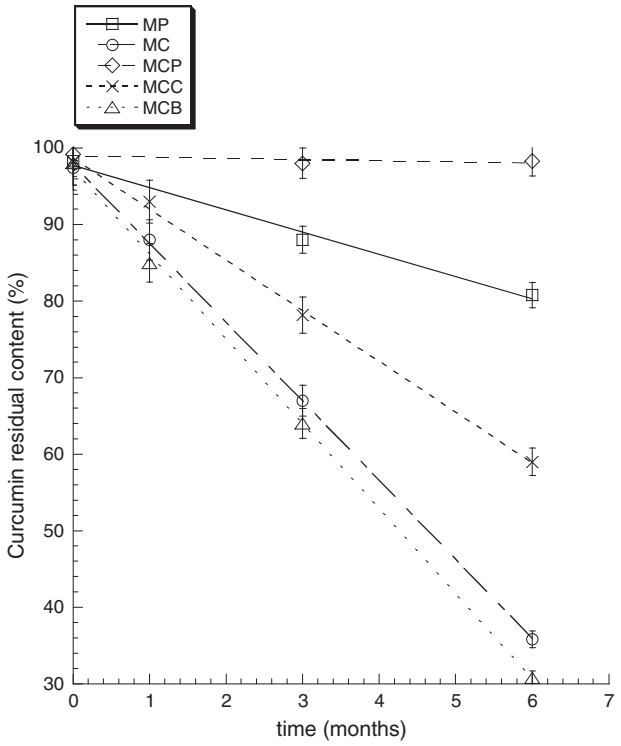

Fig. 6. Curcumin content in MAD as a function of time. Data are the means of 5 analyses on different batches of the same type of dispersions.

It is interesting to note the absence of burst release in both profiles, whereas a lag time can be observed in the first 2 h, followed by a biphasic release almost linear up to 24 h. The sustained release of hydrophobic molecules from cubosomes was found also by other authors [43].

3.4. Mathematical analysis of CR release modalities

The theoretical release curves were determined according to the linear form of Eq. (1), mimicking a dissolutive model and Eq. (2), mimicking a diffusive model [23,44]. In Fig. 7 the comparison between the theoretical curves calculated from Eqs. (1) and (2) and the experimental curves obtained for MP (Fig. 7B) and MCP (Fig. 7C) is reported. Table 4 reports the parameters (K, c and R) determined by linearization of release rate data.

The experimental curves reported in Fig. 7B and C are superposable to the theoretical curves calculated from Eq. (1), referring to dissolutive kinetics.

From the values reported in Table 4, it is confirmed that CR release from both MAD appears to be more consistent with kinetics of the dissolution rather than of the diffusion type, on the bases of the higher value of R found in the case of linearization of Eq.(1). As found by other authors, in the case of poor soluble molecules the controlling factor for release from cubic phases is dissolution rate rather than diffusion rate [45].

3.5. Production and characterization of viscous forms

In order to obtain vehicles suitable for possible administration on the skin, the low viscosity of the MAD was adequately improved by the use of xanthan gum.

Viscosity values of CR-MAD ranged between 861 and 1457 cP, at a shear rate value of 10 s^{-1}, as reported in Table 5. The highest value was obtained by CR-MCB x-gum and the lowest by CR-MP x-gum. The presence of different nanosystems in the MAD could account for the differences in viscosity.

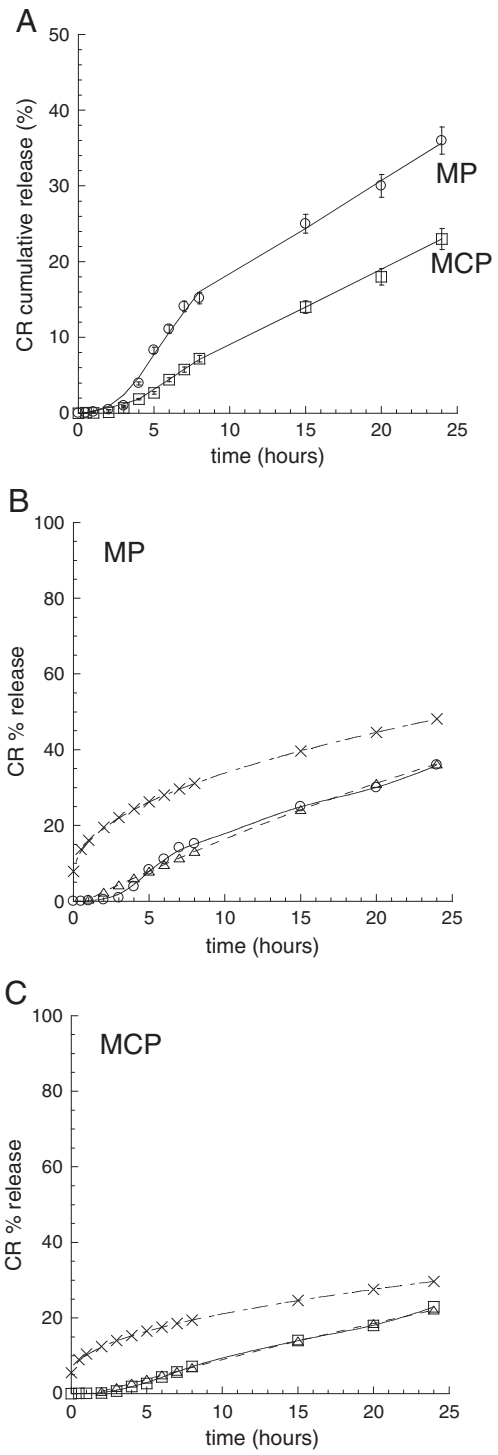

Fig. 7. (A) CR release profiles from MP and MCP obtained by modified Franz cell. Data represent the mean of 4 independent experiments ± S.D. (B and C) Comparison of the theoretical (dotted lines) and experimental (solid lines) CR profiles from MP and MCP. The theoretical curves were obtained using the coefficient calculated by linear regression of the linearized form of Eq. (1) (triangles) and Eq. (2) (crosses).

Plain xanthan gum (1% w/w) in water has a viscosity of 400 cP in the presence of CR.

3.6. In vitro drug diffusion through SCE membranes

Since previously it was found that MP was able to control the diffusion of indomethacin by cutaneous administration [46], the in vitro CR

Table 4
Kinetic parameters of CR release from CR-MP and CR-MCP.

Acronym	Equation	*K*	*c*	*R*
CR-MP	$Mt/M\infty = K_{Diss}t^{0.5} + c$	−0.019364	4.6191	0.99152
	$1 - Mt/M\infty = e - {}^{Kt}_{Diff} + c$	8.2028	−7.9221	0.95852
CR-MCP	$Mt/M\infty = K_{Diss}t^{0.5} + c$	−0.011105	4.6218	0.99428
	$1 - Mt/M\infty = e - {}^{Kt}_{Diff} + c$	4.9362	−5.5039	0.93533

diffusion through SCE membranes was studied in order to investigate the efficiency of MAD designed as topical cutaneous vehicles.

In particular Franz cell was employed to compare diffusion kinetics of CR from the different MAD. CR diffusion from liquid MAD was compared with that from viscous MAD (MAD-x gum), while CR dispersed in plain xanthan gum gel (x gum) was taken as control.

Cumulative plots of the amount of CR permeated through SCE membranes as a function of time have been determined. CR steady state flux values (F_n) for the different vehicles are reported in Fig. 8 and Table 5.

The F_n of CR formulated in MC resulted the highest among the obtained data, followed by MCB. MCP and MCC displayed intermediate and similar values, while MP exhibited the lowest F_n.

The differences in F_n may be ascribed to the type of nanostructure present in the MAD disperse phase and to the interaction between CR molecules and the disperse phase.

CR diffuses rapidly from MC and MCP which are mainly constituted of vesicles and few structured inner particles. The lower CR fluxes from MCB and MC could be justified by the presence of different structural systems (i.e. cubosomes, hexasomes and vesicles with invaginations) which could slow CR diffusion. Eventually the presence of poloxamer vesicles and ordered cubosomes, could better control CR diffusion from MP, resulting in the slowest F_n.

In the case of MAD-x gum, F_n trend was almost the same, with lower values with respect to the corresponding liquid MAD. The plain vehicle (x-gum) demonstrated the highest F_n, while the presence of monoolein based nanosystems resulted in a decrease of F_n. This result indicates that nanoparticulate structures, as well as vehicle viscosity, can control CR diffusion.

Statistical analysis revealed significant differences ($p < 0.01$) between F_n values obtained for all MAD formulations.

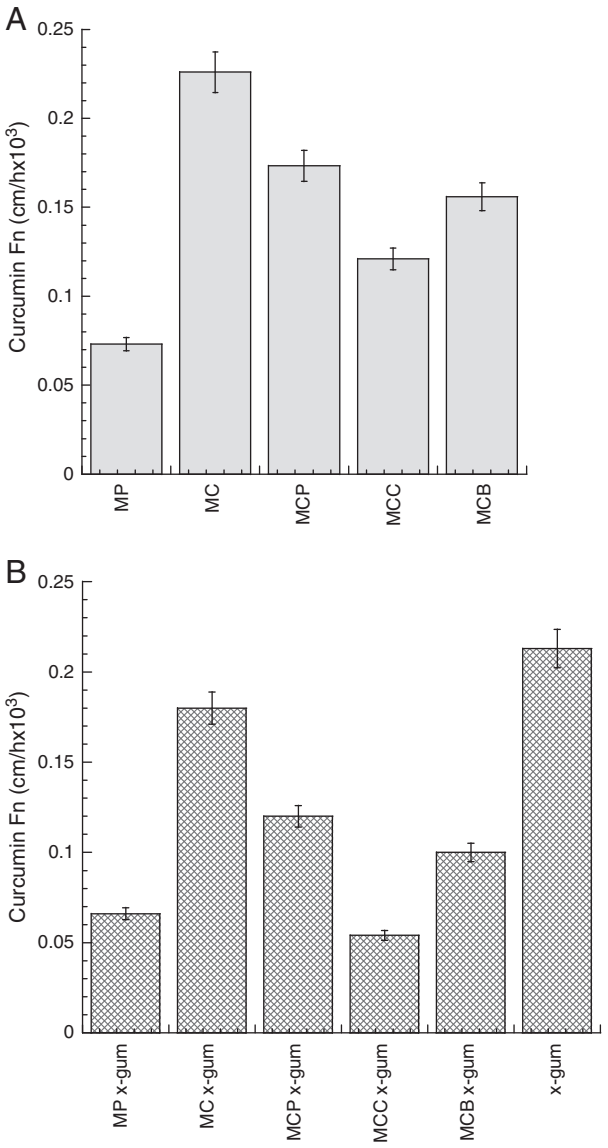

Fig. 8. Steady state fluxes (F_n) of CR from liquid (panel A) and viscous (panel B) MAD. In panel B, the F_n value of CR from xanthan gum is also reported. Data represent the mean of 5 independent experiments ± S.D.

4. Conclusions

This study indicates that selection of emulsifiers is a crucial point in the obtainment of MAD.

Apart from the largely employed poloxamer, other natural components differently contribute with monoolein to nanostructure formation. In particular the sole Na cholate or the sole Na caseinate added to monolein produces only vesicles (diffuse scattering by x-ray) while the addition of CR or poloxamer to the emulsifier promotes formation of *Pn3m* phase. The association of Na cholate and Na caseinate leads to the formation of different structures with a predominance of hexagonal phases. Lastly, the use of bentonite with Na cholate results in both *Pn3m* and *H* phases.

In all cases CR is almost completely associated to the disperse phase of MAD, as evidenced by SdFFF. Stability tests showed that MAD are able to control MAD degradation, in particular MCP maintains 98% of CR concentration also after 6 months.

Franz cells associated to dialysis membrane indicated that MP and MCP could be suitable for CR subcutaneous administration, suggesting a dissolution releasing mode of CR.

Franz cell associated to SCE membranes suggested that CR diffusion is affected by MAD composition. Moreover x-gum based MAD better restrain CR fluxes with respect to plain x-gum and to liquid MAD.

The encouraging results obtained by MCP (i.e. the high CR encapsulation efficiency and the maintenance of stability) suggest to thoroughly investigate its use for CR administration.

Table 5
Viscosity, pH and Fn values of CR-MAD[a].

Acronym	Viscosity (cP) at 10 s^{-1}	pH	Fn (cm/h × 10^3)
CR-MP	n.d.	6.49 ± 0.01	0.073 ± 0.01
CR-MC	n.d.	7.16 ± 0.02	0.226 ± 0.03
CR-MCP	n.d.	6.44 ± 0.01	0.173 ± 0.02
CR-MCC	n.d.	7.18 ± 0.02	0.121 ± 0.01
CR-MCB	n.d.	8.02 ± 0.03	0.156 ± 0.02
CR-MP x-gum	861 ± 15	6.12 ± 0.01	0.066 ± 0.01
CR-MC x-gum	1282 ± 11	6.95 ± 0.02	0.180 ± 0.02
CR-MCP x-gum	1146 ± 24	6.29 ± 0.02	0.120 ± 0.02
CR-MCC x-gum	1214 ± 15	6.71 ± 0.01	0.054 ± 0.01
CR-MCB x-gum	1457 ± 22	7.61 ± 0.02	0.100 ± 0.01
CR-x-gum	400 ± 10	6.00 ± 0.01	0.213 ± 0.02

Data represent the mean of 5 independent experiments ± S.D.
n.d.: not determined.
[a] MAD produced in the presence of curcumin.

Acknowledgements

The authors are grateful to Dr. Alice Zanellati and to Dr. Anna Bianchi for technical help.

Appendix A. Supplementary data

Supplementary data to this article can be found online at http://dx.doi.org/10.1016/j.msec.2013.08.017.

References

[1] A.M. Anderson, M.S. Mitchell, R.S. Mohan, Isolation of curcumin from turmeric, J. Chem. Educ. 77 (2000) 359–360.
[2] I. Chattopadhyay, K. Biswas, U. Bandyopadhyay, R.K. Banerjee, Turmeric and curcumin. Biological actions and medicinal applications, Curr. Sci. 87 (2004) 44–50.
[3] B.B. Aggarwal, K.B. Harikumar, Potential therapeutic effects of curcumin, the anti-inflammatory agent, against neurodegenerative, cardiovascular, pulmonary, metabolic, autoimmune and neoplastic diseases, Int. J. Biochem. Cell Biol. 41 (2009) 40–59.
[4] J.S. Jurenka, Anti-inflammatory properties of curcumin, a major constituent of *Curcuma longa*: a review of preclinical and clinical research, Altern. Med. Rev. 14 (2009) 141–153.
[5] S.H. Jee, S.C. Shen, C.R. Tseng, H.C. Chiu, M.L. Kuo, Curcumin induces a p53-dependent apoptosis in human basal cell carcinoma cells, J. Invest. Dermatol. 111 (1998) 656–661.
[6] R.L. Thangapazham, A. Sharma, R.K. Maheshwari, Beneficial role of curcumin in skin diseases, Adv. Exp. Med. Biol. 595 (2007) 343–357.
[7] B. Bhawana, R.K. Basniwal, H.S. Buttar, V.K. Jain, N. Jain, Curcumin nanoparticles: preparation, characterization, and antimicrobial study, J. Agric. Food Chem. 59 (2011) 2056–2061.
[8] A. Yaghmur, O. Glatter, Characterization and potential applications of nanostructured aqueous dispersions, Adv. Colloid Interf. Sci. 147 (2009) 333–342.
[9] B. Siekmann, H. Bunjes, M.H.J. Koch, K. Westesen, Preparation and structural investigations of colloidal dispersions prepared from cubic monoglyceride/water phases, Int. J. Pharm. 244 (2002) 33–43.
[10] E. Esposito, N. Eblovi, S. Rasi, M. Drechsler, G.M. Di Gregorio, E. Menegatti, R. Cortesi, Lipid based supramolecular systems for topical application: a preformulatory study, AAPS PharmSci. 5 (2003) E30.
[11] V. Luzzati, H. Delacroix, A. Gulik, T. Gulik-Krzywicki, P. Mariani, R. Vargas, The cubic phases of lipids, Curr. Top. Membr. 44 (1997) 3–24.
[12] J. Gustafsson, H. Ljusberg-Wharen, M. Almgrem, K. Larsson, Cubic lipid/water phase dispersed into submicron particles, Langmuir 12 (1996) 4611–4613.
[13] L. De Campo, A. Yaghmur, L. Sagalowicz, M.E. Leser, H. Watzke, O. Gattler, Reversible phase transitions in emulsified nanostructured lipid systems, Langmuir 20 (2004) 5254–5261.
[14] E. Esposito, P. Mariani, L. Ravani, C. Contado, M. Volta, S. Bido, M. Drechsler, S. Mazzoni, E. Menegatti, M. Morari, R. Cortesi, Nanoparticulate lipid dispersions for bromocriptine delivery: characterization and in vivo study, Eur. J. Pharm. Biopharm. 80 (2012) 306–314.
[15] G. Worle, M. Drechsler, M.H.J. Koch, B. Siekmann, K. Westesen, H. Bunjes, Influence of composition and preparation parameters on the properties of aqueous monoolein dispersions, Int. J. Pharm. 329 (2007) 150–157.
[16] J. Gustafsson, H. Ljusberg-Wharen, M. Almgrem, K. Larsson, Submicron particles of reversed lipid phases in water stabilized by a nonionic amphiphilic polymer, Langmuir 13 (1997) 6964–6971.
[17] K. Larsson, Aqueous dispersion of cubic lipid/water phases, Curr. Opin. Colloid Interface Sci. 5 (2000) 64–69.
[18] P. Mariani, V. Luzzati, H. Delacroix, Cubic phases of lipid containing systems. Structure analysis and biological implications, J. Mol. Biol. 204 (1988) 165–189.
[19] R. Pecora, Dynamic light scattering measurement of nanometer particles in liquids, J. Nanoparticle Res. 2 (2000) 123–131.
[20] C. Contado, G. Blo, F. Fagioli, F. Dondi, R. Beckett, Characterisation of River Po particles by sedimentation field-flow fractionation coupled to GFAAS and ICP-MS, Colloids Surf. A: Physicochem. Eng. Aspect 120 (1997) 47–59.
[21] E. Esposito, L. Ravani, C. Contado, A. Costenaro, M. Drechsler, D. Rossi, E. Menegatti, A. Grandini, R. Cortesi, Clotrimazole nanoparticle gel for mucosal administration, Mat. Sci. Eng. C 33 (2013) 411–418.
[22] E. Toitou, B. Fabin, Altered skin permeation of highly lipophilic molecule: tetrahydrocannabinol, Int. J. Pharm. 43 (1988) 17–22.
[23] N.A. Peppas, Analysis of Fickian and non-Fickian drug release from polymers, Pharm. Acta Helv. 60 (1985) 110–111.
[24] A.M. Kligman, E. Christophers, Preparation of isolated sheets of human stratum corneum, Arch. Dermatol. 88 (1963) 702–705.
[25] C. Puglia, F. Bonina, L. Rizza, R. Cortesi, E. Merlotti, M. Drechsler, P. Mariani, C. Contado, L. Ravani, E. Esposito, Evaluation of percutaneous absorption of naproxen from different liposomal formulations, J. Pharm. Sci. 99 (2010) 2819–2829.
[26] R.L. Bronaugh, R.F. Stewart, M. Simon, Methods for in vitro percutaneous absorption studies. VII: Use of excised human skin, J. Pharm. Sci. 75 (1986) 1049–1097.
[27] M. Siewert, J. Dressman, C.K. Brown, V.P. Shah, FIP/AAPS guidelines to dissolution/in vitro release testing of novel/special dosage forms, AAPS PharmSciTech 4 (2003) E7.
[28] M. Lindstrom, H. Ljusberg-Wahren, K. Larsson, B. Borgstrom, Aqueous lipid phases of relevance to intestinal fat digestion and absorption, Lipids 16 (1981) 749–754.
[29] F. Caboi, J. Borne, T. Nylander, A. Khan, A. Svendsen, S. Patkar, Lipase action on a monoolein/sodium oleate aqueous cubic liquid crystalline phase—a NMR and X-ray diffraction study, Colloids Surf. B: Biointerfaces 26 (2002) 159–171.
[30] W. Buccheim, K. Larsson, Cubic lipid–protein–water phases, J. Colloid Interface Sci. 117 (1987) 582–583.
[31] M. Golding, A. Sein, Surface rheology of aqueous casein-monoglyceride dispersions, Food Hydrocoll. 18 (2004) 451–461.
[32] J. Zhai, L. Waddington, T.J. Wooster, M.-I. Aguilar, B.J. Boyd, Revisiting β-casein as a stabilizer for lipid liquid crystalline nanostructured particles, Langmuir 27 (2011) 14757–14766.
[33] G. Began, E. Sudharshan, K. Udaya Sankar, A.G. Appu Rao, Interaction of curcumin with phosphatidylcholine: a spectrofluorometric study, J. Agric. Food Chem. 47 (1999) 4992–4997.
[34] Y.J. Wang, M.-H. Pan, A.-L. Cheng, L.-I. Lin, Y.-S. Ho, C.-Y. Hsieh, J.-K. Lin, Stability of curcumin in buffer solutions and characterization of its degradation products, J. Pharm. Biomed. Anal. 15 (1997) 1867–1876.
[35] L.C. Price, R.W. Buescher, Decomposition of turmeric curcuminoids as affected by light, solvent and oxygen, J. Food Biochem. 20 (1996) 125–133.
[36] L.C. Price, R.W. Buescher, Kinetics of alkaline degradation of the food pigments curcumin and curcuminoids, J. Food Sci. 62 (1997) 267–269.
[37] H.H. Tonnesen, M. Masson, T. Loftsson, Studies of curcumin and curcuminoids. XXVII. Cyclodextrin complexation: solubility, chemical and photochemical stability, Int. J. Pharm. 244 (2002) 127–135.
[38] C. Puglia, V. Cardile, A.M. Panico, L. Crascì, A. Offerta, S. Caggia, M. Drechsler, P. Mariani, R. Cortesi, E. Esposito, Evaluation of monooleine aqueous dispersions as tools for topical administration of curcumin: characterization, in vitro and ex-vivo studies, J. Pharm. Sci. 102 (2013) 2349–2361.
[39] E. Esposito, S. Mazzitelli, R. Cortesi, M. Drechsler, L. Ravani, C. Nastruzzi, Analysis of the drug release profiles from formulations based on micro and nano systems, Curr. Anal. Chem. 9 (2013) 37–46.
[40] V. Venkateswarlu, K. Manjunath, Preparation, characterization and in vitro release kinetics of clozapine solid lipid nanoparticles, J. Control. Release 95 (2004) 627–638.
[41] L.C. Herrera, M.V. Defain Tesoriero, L.G. Hermida, In vitro release testing of PLGA microspheres with Franz diffusion cells, Dissolut. Technol. 5 (2012) 6–11.
[42] D.-B. Chen, T.-Z. Yang, W.-L. Lu, Q. Zhang, In vitro and in vivo study of two types of long-circulating solid lipid nano-particles containing paclitaxel, Chem. Pharm. Bull. 49 (2001) 1444–1447.
[43] H. Chung, S.Y. Jeong, I.C. Kown, Cubic liquid-crystalline particles as protein and insoluble drug delivery systems, in: M.L. Lynch, P.T. Spicer (Eds.), Bicontinuous Liquid Crystals, CRC Press, Taylor & Francis Group, Boca Raton (FL), 2005, pp. 353–385.
[44] E. Esposito, E. Menegatti, R. Cortesi, Hyaluronan based microspheres as tools for drug delivery: a comparative study, Int. J. Pharm. 288 (2005) 35–49.
[45] J. Lee, I.W. Kellaway, The controlled release of drugs from cubic phases of glyceryl monooleate, in: M.L. Lynch, P.T. Spicer (Eds.), Bicontinuous Liquid Crystals, CRC Press, Taylor & Francis Group, Boca Raton (FL), 2005, pp. 457–469.
[46] E. Esposito, R. Cortesi, M. Drechsler, L. Paccamiccio, P. Mariani, C. Contado, E. Stellin, E. Menegatti, F. Bonina, C. Puglia, Cubosome dispersions as delivery systems for percutaneous administration of indomethacin, Pharm. Res. 22 (2005) 2163–2173.